Plasma power balance: methodology and investigations of microwave capillary discharges

F Coquery, Olivier Leroy, Tiberiu Minea, G Stancu

Plasma power balance: methodology and investigations of microwave capillary discharges

F. Coquery[1,2], O. Leroy[2], T. Minea[2] and G.D.Stancu[1*]

[1]Laboratoire EM2C, CNRS, CentraleSupélec, Université Paris-Saclay, 3, rue Joliot Curie, 91192 Gif-sur-Yvette, France

[2]Laboratoire LPGP, Université Paris-Saclay,CNRS, 91405 Orsay, France

*Email: gabi-daniel.stancu@centralesupelec.fr

Abstract

Nowadays, where strong energy constraints are set by the environmental and economical context, the real power coupled in plasmas becomes a critical aspect particularly for applications where plasma technologies are facing competition. This issue is enhanced for atmospheric pressures micro-plasmas, where the local power density can be very high (e.g. $10^5 Wcm^{-3}$) which implies fast heat exchanges. The precise knowledge of the power coupled to plasma is also a key for fundamental understanding of discharge properties. This is often used as an input parameter for plasma modeling and its inaccuracy can mitigate the predictive quality of plasma simulation tools. In the present paper the macroscopic power balance was established for continuous microwave (MW) plasmas generated in capillaries in argon gas flows. The macroscopic power budgets were performed based on measurements of microwave leak fluxes, heat fluxes (thermal radiation, convection, conduction), optical radiation and chemical powers. It was proven that the traditional power measurements at the MW generator would largely overestimate the real power coupled to plasmas, namely by at least a factor two. An important power fraction is found in the heat transfer through the MW launcher, the impedance mismatching being here better assessed.The proposed methodology, which is based on the physics of transport phenomena, can be employed for characterization of other (micro-) plasma sources.

1. Introduction

Continuous wave and pulsed micro-plasma sources have shown a growing interest over the last decade due to their high potential of applications in fields such as nano-material synthesis, micro-propulsion, photonics, plasma-assisted combustion, chemical analysis and conversion, environmental, agriculture, and biomedical applications[1][2][3][4][5][6][7][8]. Surface wave discharges such as microwave capillary discharges are particularly interesting for applications because of their electrodeless configuration and great flexibility and stability in operation conditions[9],[10]. With capillary diameters down to 100 μm, large power density plasmas (up to 0.1MW cm^{-3}) can be generated by surfatron or stripline launchers in gases that ranges from mbar to atmospheric pressures[10][11][12].

The development and optimization of plasma applications require a fundamental understanding of kinetics and dynamics phenomena, as well as the energy branching and power coupling to plasmas. Especially today, where the environmental and consumption constrains are enhanced, the energy costs of plasma technologies are furthermore challenged. For MW plasmas and beyond, the key parameter θ, which represents the mean power required for one electron-ion pair production is assessed[13]. For example, in the pressure range 0.05 to 2 torr in a argon surfatron discharge with 4.5 mm tube radius, and based on a theoretical model, θ is found between $5x10^{-12}$and $2x10^{-13}$W[14]. Concerning the macroscopic power balance, namely the evaluation of the power coupled to plasmas, this is usually performed by a simple balance between incident and reflected powers that are measured at MW generator[15][16][17]. However, this procedure remains questionable. A typical MW circuit includes waveguides, bidirectional couplers, matching stubs and launchers, where most of them often present hot surfaces. This indicates that MW power is converted into heat and therefore the simple power balance that accounts for impedance mismatching is most probably inaccurate to evaluate the power coupled to the plasma. This difference can be enhanced for the micro-plasmas where the power density easily exceeds 10^5 Wcm^{-3}, for less than 100 W injected into the circuit. Moreover, one should notice that accurate knowledge of the plasma power is also important for modeling, this is often used as an input parameter, e.g.[16][18].

In this article the power balance methodology based on transport phenomena is described and applied to microwave capillary discharges generated in argon gas flows, with powers below 50W (to avoid capillary thermal damages under extensive plasma exposures), in a quartz capillary tube with internal and external diameters of 1 and 2 mm, respectively. In

section 2 the power balance method is detailed. In section 3 power balances are performed with and without plasmas including evaluations of the heat fluxes based on measurements with infrared (IR) camera, thermocouples and temperature sensitive papers; of the optical flux based on calibrated optical emission spectroscopy; of the Ar metastable flux using Tunable Diode laser Absorption Spectroscopy (TDLAS) and of the microwave leak flux using electromagnetic (EM) probes. The article conclusions are presented in section 4.

2. Power balance methodology

2.1 Fluxes and power components

The power balance methodology is based on the principle of the energy conservation in a steady state system. In case of no heat generation inside the system, the algebraic sum of fluxes that enter and exit the system surface should be zero[19]:

$$-\oiint \vec{\varphi} \cdot \vec{n}\, dS = 0,$$

where $\vec{\varphi}$(Wm^{-2}) represents fluxes of different natures and $\vec{n}$ is the normal vector oriented externally to the system.

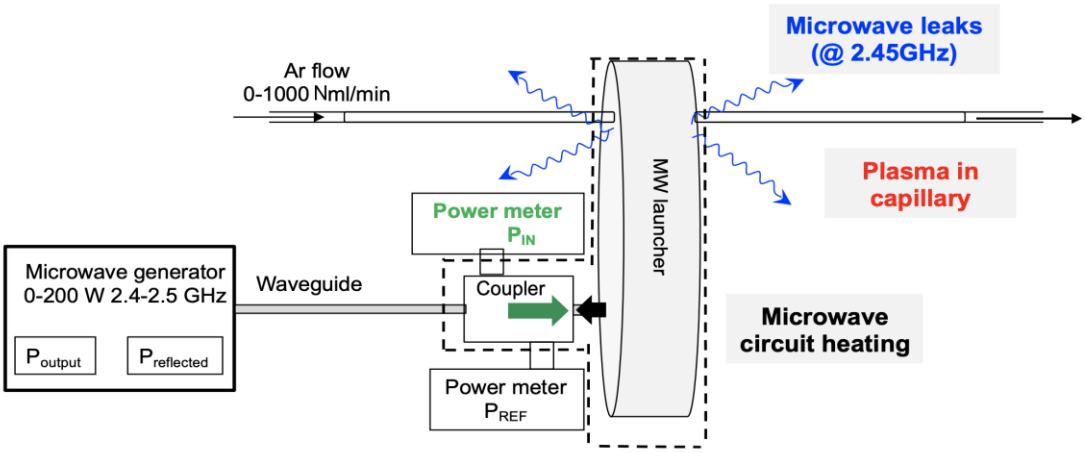

Figure 1. Schematics of the microwave capillary discharge set-up. The power difference (P_{IN} -P_{REF}) measured close to MW launcher is shared into the heat dissipated by the microwave circuit, the capillary plasma and microwave leaks.

When the plasma system (see Figure 1), which includes here the capillary plasma and the MW circuit (includes a surfatron or microstrip laucher and a bidirectional coupler) reaches the steady state regime, the MW power that enters the system is transformed and branched in several channels:

- (1) inside the MWcircuit the EM field will heat up the metallic conductive surfaces

- (2) at the gap location (space between capillary and launcher) the MWcan leak outside
- (3) when plasma is ignited, the MW power is transferred to the surface wave at the capillary interface that will accelerate the electrons, the plasma being the medium in which the surface wave propagates. The energy gain by the electrons will be transferred through elastic and inelastic collisions to heavy particles and to the capillary surface. Hence the plasma power is finally transferred outside as:
    - 3a) heat power across the capillary walls
    - 3b) heat power in the gas which exits the capillary
    - 3c) power in chemistry or in excited species which exits the capillary
    - 3d) radiative power transferred through the spectral windows for which the capillary is transparent.

The first power term (1) can be determined as follows. The launcher is an opaque body for which at the interface the continuity of fluxes gives[19]:

$$\varphi^{CD} = \varphi^{CC} + \varphi^{R}, \qquad (1)$$

Namely the conductive flux that diffuses inside the launcher material is transferred to the environment by phenomena of conduction coupled to convection and thermal radiation. The radiative flux can be computed for an isotropic gray body of emissivity ε, surrounded by a large room with walls at constant temperature, T_{wall}, as:

$$\varphi^{R} = \varepsilon\sigma(T^4 - T_{wall}^4), \qquad (2)$$

where σ denotes Stefan's constant. The conducto-convective flux, which represents the exchange with air at T_{air} is given by:

$$\varphi^{CC} = h\,(T - T_{air}), \qquad (3)$$

where h(Wm^{-2}K^{-1}) is the exchange coefficient that depends on the type of convection, fluid nature and geometry. This coefficient can be determined using correlations from the literature. Thus, by measuring the temperatures of the launcher external surface and the room walls, and by integrating the two fluxes over the launcher surface, the power spent directly in heating the launcher can be assessed.

The second term (2) can be evaluated using an EM probe that measures the MW flux over a virtual box, which surrounds the launcher. Integrating the flux over the box surface will give the power lost at MW frequency, namely at 2.45GHz.

The real power coupled to plasma, term (3), can be determined as follows. The part 3a), the heat power across the capillary is evaluated using the same method as for the term (1). The difference stands in evaluation of h, which here is specific for the capillary (i.e.

cylindrical) horizontal geometry, and for assessment of the radiative thermal flux, which is here specific for a non-gray body. We should note that the quartz capillary is practically an opaque body for the thermal radiation. Because the external surface temperatures are usually in the range 293 K to 400 K, more than 98 % of the Planck radiation is in the wavelength range of 3.6 μm to79 μm. The quartz transmissivity drops from 0.8 to 0 from 3.6 μm to 4.8 μm respectively [20]. A significant transmittance for 1 mm quartz thickness (e.g. 0.1) is observed for wavelength higher than 40 μm [21]. However, the capillary remains practically opaque for the thermal radiation in our experiment. Note that the black body radiation (for this temperature range) transmitted in the spectral windows below 4.8 μm and higher than 40 μm is about 5 %.

Yet, the surface emissivity is not gray but changes with wavelength, therefore the radiative flux need to be evaluated using the Planck intensity, I_λ^o, as:

$$\varphi^R = \pi \int \varepsilon(\lambda)[I_\lambda^o(T) - I_\lambda^o(T_{wall})]d\lambda. \qquad (4)$$

By measuring the capillary external surface temperature and then by integrating φ^R and φ^{CC} over the capillary surface up to locations (upstream and downstream of the plasma) where the temperature is about the room temperature, this power term is then evaluated.

Note that the capillary exit location is chosen to be the post discharge region (no plasma light emission), but which may contain excited states, chemical compounds, and gas heat. The term 3b), the heat power in the gas at capillary exit can be determined as:

$$P_{gas} = \dot{m}\, c_p \Delta T, \qquad (5)$$

where $\dot{m}$(kg s^{-1}) is the gas mass flow rate, $c_p$is the gas heat capacity ($Jkg^{-1}K^{-1}$), and ΔT is the gas temperature difference from entrance to exit. By placing thin thermocouples at capillary entrance and exit locations, one can then determine this power fraction.

The 3c) term, the power in chemistry or excited species at capillary exit can be easily evaluated when the discharge is ignited in rare gases. For instance, in our case of Ar post-discharge, no chemical species are present. The only non-radiative states that may live particularly at low pressure are argon metastables. These species concentration, $n_{Ar^{met}}$, can be measured using resonant absorption spectroscopy, such as Tunable Diode Laser Absorption Spectroscopy (TDLAS)[22].The power contained in the metastable flux is then given by:

$$P_{Ar^{met}} = n_{Ar^{met}}\, v\, A\, E_{Ar^{met}}, \qquad (6)$$

where v is the flow speed, A the cross-section area of the capillary, and $E_{Ar^{met}}$ is the metastable internal energy.

The 3d) term, the radiative power transferred in the transparent spectral window of the capillary can be determined using a calibrated optical emission measurement. The quartz is transparent in the window 0.2 μm to 3.6μm. The VUV and Mid-IR radiation of plasma are absorbed by the capillary and then converted in the conductive flux. The spectral isotropic emission coefficient of plasma, $\xi_\lambda(Wm^{-3}sr^{-1}nm^{-1})$, can be assessed from the line-of-sight measured intensity, $I_\lambda(Wm^{-2}sr^{-1}nm^{-1}) = \int \xi_\lambda \, dl$. The intensity must be recorded perpendicularly on the capillary and from a cylindrical volume aligned to the collection direction with a radius at least ten times smaller than the capillary radius. This guarantees the emission length to be the internal diameter of the capillary and it allows to determine an averaged value of ξ_λ. Prior to this, the intensity spectrum recorded in arbitrary units (*counts/s*) is converted in absolute units ($Wm^{-2}sr^{-1}nm^{-1}$) using a calibrated source, such as tungsten lamp that is placed at the same location as plasma, insuring the same solid angle for the photon collection. By recoding the intensity at different location along the capillary (to account for axial non uniformity of plasma), the averaged plasma emission coefficient can be calculated, and the radiative power can be computed by spectral and volume integrations, as:

$$P_{RAD} = 4\pi \iint \xi_\lambda \, d\lambda \, dV. \qquad (7)$$

2.2 Conducto-convective heat transfer coefficient

The exchange coefficient, h(Wm^{-2}K^{-1}), is necessary to determine the conducto-convective flux. This can be evaluated by employing thermal correlations that are obtained experimentally or numerically using dimensionless numbers. h is given by[19]:

$$h = \frac{Nu\ \lambda}{L_c}, \qquad (8)$$

where Nu is the Nusselt number, λ(Wm^{-1}K^{-1}) is the thermal conductivity of air and L_c is a characteristic length. The correlations employed here for the natural external convection are specific for the geometry of each surface comprising the capillary, launcher, bidirectional coupler and N type connectors. These components can be considered as an assembly of horizontal cylinders, vertical and horizontal planar surfaces submitted to the natural convection phenomenon.

For a horizontal cylinder of diameter D[23]:

$$Nu = \left[0.6 + \frac{0.387 Ra^{1/6}}{\left(1+0.721 Pr^{-9/16}\right)}\right]^2 \qquad (9)$$

where Ra is the Rayleigh number given by:

$$Ra = \frac{g\beta\,(T-T_{air})D^3}{va} \qquad (10)$$

with g the standard gravity, $\beta = 1/T_f$ for an ideal gas, where the film temperature, T_f, is defined as$T_f = \frac{T_{surface} + T_{air}}{2}$, ν and a are air mechanical and thermal diffusivities taken at the film temperature, respectively. The Prandtl number, Pr, is given by $Pr = \nu/a$. This correlation is valid for $10^{-5} < Ra < 10^{12}$.

Here the diameters of cylindrical elements range between 0.2 cm for the capillary and 10 cm for the plasma launcher. Taking a typical surface temperature of 30 °C for the launcher and the surrounding air at temperature of 20 °C, we find $Ra \sim 10^6$, whereas for the capillary with a typical surface temperature of 130 °C we obtain $Ra \sim 36$. Thus, the above criterion is verified.

For a vertical plane of height *H*[24]:

$$Nu = \left[0.68 + \frac{0.67 Ra^{1/4}}{\left(1+0.671 Pr^{-9/16}\right)^{4/9}}\right], \qquad (11)$$

This correlation is valid for an isothermal wall in laminar convection, so for the Grashof number, Gr:

$$Gr = \frac{g\beta\,(T - T_{air})H^3}{\nu^2} < 10^9. \qquad (12)$$

Note that verticals planes are here less than 10 cm length. For this we get $Gr \sim 10^6$, which confirms the laminar regime for the natural convection.

For an isothermal horizontal plane of length *L*, a hot wall facing upward[25]:

$$Nu = 0.54\, Ra^{1/4}. \qquad (13)$$

This correlation is valid for $Pr > 0.5$ and $10^4 < Ra < 10^7$.

For an isothermal horizontal plane of length *L*, a hot wall facing downward[26]:

$$Nu = 0.27\, Ra^{1/4}. \qquad (14)$$

This correlation is valid for $Pr > 0.5$ and $10^5 < Ra < 10^{10}$.

The latter criteria are valid as well, because for air at room temperature $Pr \sim 0.7$ and $Ra < 10^7$. The thermophysical properties of air versus the temperature are taken from reference [27].

2.3 Characteristic times and steady state regime

The time necessary to reach the steady state regime is determined by the slowest thermal phenomenon. This can be estimated using the characteristic times. The conduction time or the heat diffusion time inside materials employed, can be computed using, $\tau^{CD} = \frac{x^2}{a}$, where *x* is the characteristic thickness and *a* is the characteristic thermal diffusivity. For

example, for 1 *cm* thickness of aluminum, static air, quartz and teflon, it corresponds to1*s*, 5*s*, 2 *min* and 13 *min*, respectively.

The characteristic time for heat exchanges between the solid surface and the environmental air, which is the conduction coupled to convection phenomenon can be computed by, $\tau^{CC} = \frac{\rho\ cp\ V}{h\ S}$, where ρ is the mass density, *cp* is the heat capacity, *h* is the conducto-convective exchange coefficient, *V* and *S* are volume and surface of the solid, respectively. For an aluminum cylinder of radius 5 cm and thickness of 2 cm placed in natural convection, τ^{CC} is about 30*min*.

The radiative exchange between a solid surface and the walls of the experimental room, in case of $\Delta T/T << 1$, is a slow process. Its characteristic time can be computed using the same expression with *h* being the radiative exchange coefficient. Because the radiative and the natural convective coefficients are about the same, their characteristic time are also similar. Note that if the surface is at significantly higher temperature compared to building walls, then the characteristic time will be shorter. The same occurs also if the solid surface is placed in forced convection, namely τ^{CC}becomes shorter.

Note that thermal steady state conditions are achieved when running the system for a duration of a fewtimes the longest characteristic time. For the system configurations studied here, this can be on the order of two hours.

2.4 Impedance matching: power coupled to the system

The MW power coupled to the system or even to the plasma is traditionally established from the difference P_{output} - P_{input}, measured at the generator (see figure 1). However, as shown later, measurements of the reflected power even after a short length wave guide (coaxial cable) could be significantly underestimated. A more appropriate solution is to employ a bidirectional coupler equipped with powermeters, which allows measurements closer to the launcher. The reflected power due to impedance mismatching can be better evaluated and thus, the power transmitted to the launcher and further to the plasma is accurately assessed.

3. Results

3.1 Emissivity and temperature measurements

To ensure that the surface of the launcher is a gray diffusive body, so to have a wavelength and directional independent emissivity, we deposited on its surface a graphite thin layer (Kontaktchemiegraphit 33). The emissivity of the graphite is given as $\varepsilon = 0.95$[28].

Note that this is the largest and hottest part among the metallic components, i.e. a cylinder with diameter of 11.4 cm and length of 2.8 cm.

The bidirectional coupler is a parallelepiped of 5.4 x5.1 x2.2 cm^3 made of aluminum, whereas the N-type connectors are made of stainless steel, they can be considered as six consecutive cylinders of 1.6; 2.1; 1.7; 2.1; 1.7; 0.9 *cm* and 0.9; 1.7; 0.7;1.7; 0.9; 1.2 *cm*, diameters and lengths respectively, with the range of emissivity $\varepsilon \in (0.04; 0.4)$[29].

The spectral emissivity of the quartz capillary surface, $\varepsilon(\lambda)$, varies between 0.4 to 1 in the spectral window 3 to 50 μm [30]. By spectral integration within these limits more than 95 % the thermal radiation flux is then evaluated.

The air temperature was measured using thermocouples (Omega engineering, type K) of 50μm diameter. The errors provided by the fabricant are $\pm$ 0.5 °C. They were employed also to measure the surface temperature of the launcher, bidirectional coupler and N-type connectors. As the thermal contact is far to be perfect and surrounding temperatures (air, room walls) are always lower than the surface temperatures that are evaluated, the values given by the thermocouple are systematically underestimated. We considered therefore an uneven error of -0.5°C/+1°C.

The temperature of the bidirectional coupler surface was found uniform with variations below 0.5 °C. The temperatures of the cylindrical elements that compose the N-type connectors, were found uniform, however with a difference up to 5°C between the most distant elements. The launcher surfaces, a cylinder closed by two metal disks, were found uniform with variations inside the same surface below 0.5°C and a maximum a few degrees between these surfaces.

The gas temperature in the post-discharge at exit of the capillary was measured using the same thermocouples. Their presence showed a negligible impact on the argon flow, the pressure measurements upstream and downstream remaining unaffected.

The measurements of the capillary surface temperature are particularly difficult. Its reduced diameter implies a large curvature and thus an imperfect contact with the thermocouple. In addition, the thermocouple perturbs the propagation of the surface wave, and thus modifies the plasma volume. The temperatures were therefore measured using an infrared camera (FLIR i7), which collect photons in the spectral range of 7.5 to 13 μm. However, the spectral emissivity of the capillary in this spectral range is strongly wavelength dependent, i.e. it changes in the range of 0.5 to 1 [30], whereas the camera allows to input only a constant emissivity.

To calibrate the camera for the emissivity changes the following experiments were performed. A quartz tube of large diameter, namely 10 *cm*, heated from inside using an air blower was placed in ambient air. Its temperature on the external surface was measured at same locations using thermocouples, IR camera and thermal papers (Omega, TL-8 and TL-10). The tube was heated to reach the temperature range that the IR camera will measure when aiming the capillary surface with plasma on.

In figure 2 over sixty measurements at the same location and for gradually cooling the quartz surface are made using the thermocouple and the IR camera for which an arbitrary emissivity $\varepsilon = 0.8$ was considered. We observe here systematic lower values for the thermocouple, which are due to the imperfect thermal contact. Please recall that the thermocouple measures its own temperature, which is determined after the establishment of the steady regime, by the flux amplitudes (conduction, conducto-convection and radiation) and by the corresponding thermocouple surfaces offered to each particular flux. A perfect thermal contact is achieved in case the thermocouple is completely immersed in an opaque environment. A ball-type thermocouple placed on a cylindrical quartz surface and in a lab setting will obviously not satisfied this required.

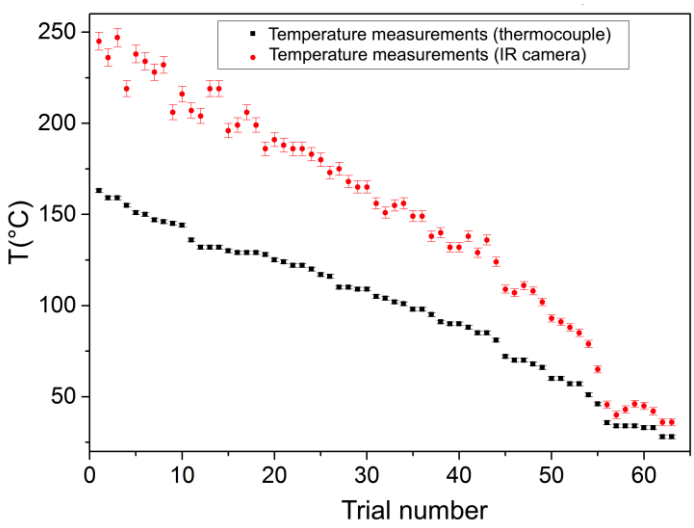

Figure 2. Temperature measurements using a thermocouple (black) and an IR camera (red) of the surface of a quartz tube of 10 cm diameter.

In figure 3 temperature measurements are made using thermal papers and the IR camera following the same procedure. The thermal contact being significantly improved for thermal papers (very thin objects with large contact surfaces), we observe a much better agreement between measurements. These temperatures are plotted against each other in figure 4. The linear fit is used further as a correction factor to adjust the temperature values

given by the IR camera, for which, as mentioned, an arbitrary constant emissivity was considered.

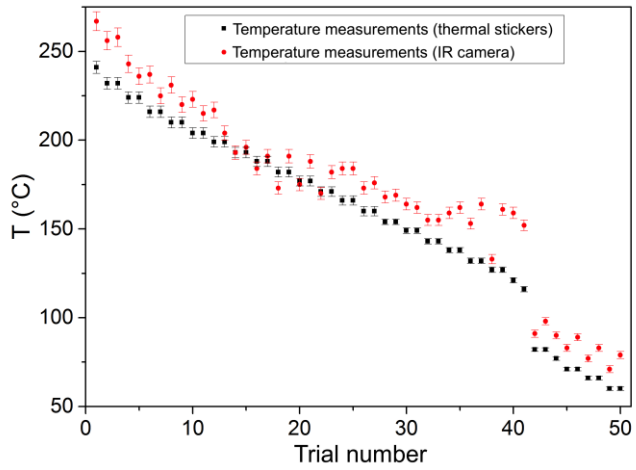

Figure 3. Temperature measurements of the surface of a quartz tube of 10 cm diameter using thermal papers - stickers (black) and an IR camera (red).

One should note that the capillary temperature is not entirely accessible to the IR camera. This because it is partially covered by the launcher over a few centimeters. The capillary temperature for this part was extrapolated from the measured values, which were obtained after the plasma was switched off, the launcher was axially translated and so the hidden part was exposed to the IR camera. This measurement was performed about one or two seconds after plasma stopped.

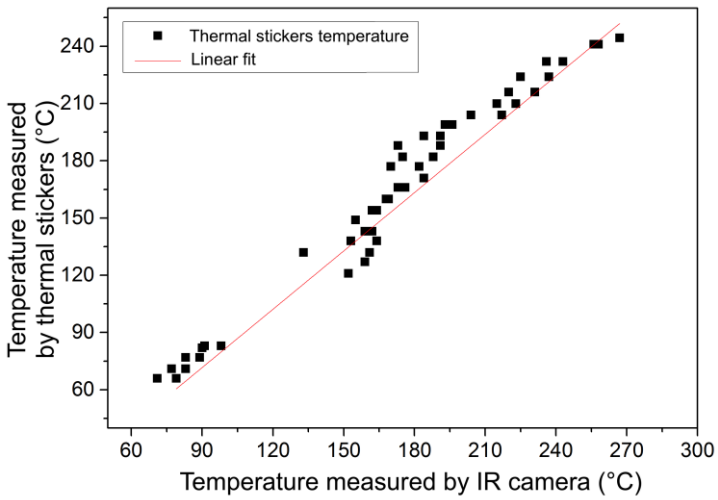

Figure 4. Correlation between the temperature measured by thermal papers (stickers) and the temperature measured by IR camera.

To estimate the temperature in steady state, i.e. before switching off the plasma, the time evolution of the surface temperature in this covered region was monitored. Experimentally, the characteristic cooling time (*1/e*) was found to be about 6 s. This can be roughly understood by a simplified 0D thermal model. For an elementary cylinder of length *dl*, cooled by the natural conducto-convection with ambient air, e.g. $h = 18\,W/m^2/K$, one can estimate the upper limit for the cooling characteristic time, to be $\tau = \frac{V\ \rho\ c_p}{h\ S} \sim 50s$, where V and S are the volume and surface, respectively, ρ and *cp* the mass density and heat capacity, respectively. However, the fast displacement of the launcher will induce external forced convection. In addition, the cooling is enhanced in parallel by the radiative exchange with room cold walls and by the forced internal convection with the argon flow. Therefore, the capillary temperature drops faster.In figure 5 the capillary surface temperature function of the axial position is presented. The red bars correspond to extrapolated values.

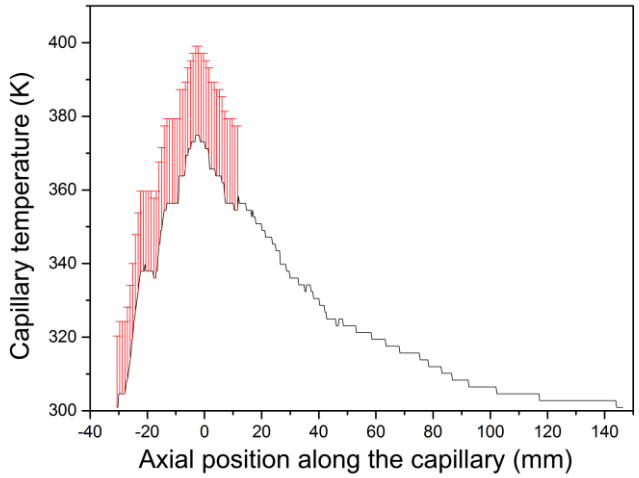

Figure 5. Capillary temperature measurements along axial position. The red bars correspond to extrapolated values, i.e. the region covered by the launcher.

3.2 Microwave power coupled to the system

As mentioned, the microwave power coupled to the system composed by the launcher and the capillary was measured using a bidirectional coupler equipped with powermeters and placed near the launcher. The microwave generator employed here was the SAIREM GMS200WSM56, which output power is adjustable in steps of 1W with a maximum of 200W and the frequency tunable in the range of 2400 to 2500 MHz in steps of 0.1MHz. The generator measures the reflected power with a resolution of 1W as well. The microwaves are

transmitted through a coaxial cable of 1.5 m and 50-Ohm impedance. At the cable end a bidirectional coupler, MECA Electronics, 722N-30-3.100, is connected to the MW launcher. The coupler has 30(±1.2) dB attenuation on measurement channels. Two powermeters, Minicircuits PWR-6GHS, were placed on each measurement channel. They work in the range of -30 dBm to 20 dBm, with a typical uncertainty of ±0.15 dBm and a maximum uncertainty ±0.3 dBm for the power range of present measurements.

In figure 6, incident and reflected powers components were recorded using a surfatron launcher to generate plasma in pure argon at flow rate of 500 Nml/min (N stands for normal conditions: 1 atm and 0 °C) at constant microwave frequency of 2427 MHz (ensuring the best impedance matching) and changing the generator input power from 2W to 50 W. No impedance matching device was employed for these measurements. It can be seen that measurements of the incident power are relatively close for the two methods, at most a difference of 5% is observed. The systematic lower measurement given by the powermeter is explained by the power losses along the coaxial cable and connections that may occur between the two measurement locations, i.e at generator and at bidirectional coupler. Note that the cable has a typical attenuation of 0.1 dB.However, the difference is significantly larger for the reflected power. For instance, at 50 W setpoint power, the generator indicates 3 W of reflected power, whereas the powermeter at the coupler gives 12W.

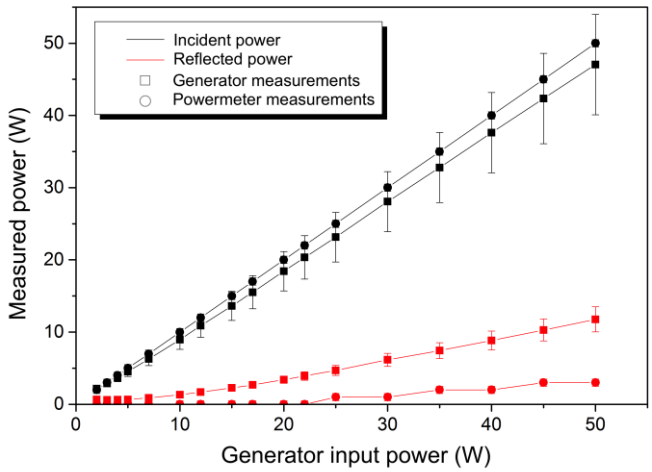

Figure 6. Measured powers (incident black, reflected red) at locations of the bidirectional coupler (squares) and of the MW generator output (circles) as a function of the generator set-point power values.

Overall, this difference is larger for higher values of the setpoint power and is explained by additional losses along the wave guide, which includes the coaxial cable and the

path inside the generator up to the measurement point. Thus, the reflected power is underestimated if measurements are performed at the generator location. This difference could be attributed also to an imperfect impedance matching of the coupler. Yet, the very small difference between the incident power measured by the generator and the powermeter confirms that the impedance of the bidirectional coupler is 50 Ω.

So, while a measurement at the generator can give us a coupling, $(P_{inp} - P_{ref})/P_{inp}$, over 95%,close to the values traditionally given in the literature (e.g. [10], [31]), the powermeters located at the launcher show this coupling being around 70% to 85%. The impedance matching is therefore overestimated by power indication (measurements) at the generator, which is commonly reported in the literature. One should note that these numbers do not reveal the effective power coupled in the plasma, as it will be established later.

These effects are also observed independent of the type of launcher used (strip-line, surfatron). The set-up configuration employed without plasma generation was the following: MW generator output power (P_{output}) 15W; MW frequency 2.45 GHz, argon flow of 300, 500 and 700 Nml/min; upstream pressure ~ 100 mbar; downstream pressure ~ 10 mbar. The powers recorded at the bidirectional coupler where 16.03; 15.86; 16.07 W and 14.11; 13.96; 14.19 W for the incident and reflected powers, respectively. The about 1W measured in addition for the incident power is explained by the precision of the generator (i.e.$\pm\, 1W$). We observe that a fraction of about 88% is reflected back to the generator and 12% only enters the launcher. This last part will heat up the launcher and would be found in MW leaks at the launcher gap hole.

However, we should note that these fractions do not consider the uncertainties of the powermeters and the attenuations of the bi-directional coupler. The attenuators have $30(\pm 0.3)\ dB$ which corresponds to $\pm$ 7 % uncertainties. Moreover, if one considers the case of + 6 % for reflected power and – 6 %for incident power, the balance will indicate total reflection.

For the same conditions except that the plasma is ON, the powers recorded at the bidirectional coupler where 15.11; 14.9; 15.07 W and 3.9; 4.3; 4.84 W for the incident and reflected powers, respectively. We observe here that the coupling in presence of plasma is not optimal, i.e. about 26 % to 32 % of incident power is reflected.

Again, if one considers the extreme uncertainties, the reflected power will range in the window of 20% to 40 %. Thus, this is clearly not the major fraction loss in the power balance.

3.3 Heat dissipated by the launcher, bi-directional coupler and N-type connections

As explained above, a fraction of the MW power that enters the launcher will not create the plasma, but it will heat up the MW circuit which is transferred to the environment (air, lab walls) by conducto-convective and thermal radiative fluxes.

In steady state, in the absence of plasma, the temperature elevation is in the range of 5 to 8 °C above the ambient temperature for the coupler and connectors, and 2 °C for the launcher. In table 1 the percentage of powers for each element is given for three Ar flows used. It was found that the launcher dissipates the most, although its temperature elevation remains relatively small, but it has the largest surface.

Ar flow	Power	Launcher (%)		Coupler (%)		N connectors (%)	
Nml/min	*W*	φ^{CC}	φ^{R}	φ^{CC}	φ^{R}	φ^{CC}	φ^{R}
300	0.84	18.1	35.1	30.2	1.3	14.5	0.7
500	0.9	19.1	36	29.3	1.4	13.5	0.7
700	0.87	19.6	36.9	27.7	1.3	13.8	0.7

Table 1. Plasma off, the dissipated power and the percentage of each element of the microwave circuit and for the fluxes, namely conducto-convective flux (φ^{CC}) and radiative flux (φ^{R}).

In the presence of plasma, the temperature elevations are significantly higher, namely 5 °C for the coupler, 6 to 11°C for the connectors, and 10 °C for the launcher. As the transmitted power through the system is much higher, there is more energy available to heat-up the MW circuit. In table 2 the percentages of powers for each element is given for the same three Ar flows, as in table 1. Comparing the three elements, it comes out that the strip-line launcher dissipates this time almost all the power. Note that all metallic surfaces dissipate about 3.6 W, which corresponds to about 24 % of the incident power.

Ar flow	Power	Strip-line (%)		Coupler (%)		N connectors (%)	
Nml/min	*W*	φ^{CC}	φ^{R}	φ^{CC}	φ^{R}	φ^{CC}	φ^{R}
300	3.47	39.2	50.5	6.3	0.3	3.5	0.2
500	3.77	38.2	49.3	8	0.3	4	0.2

700	3.58	36.8	48	10	0.4	4.5	0.2

Table 2. Plasma on, the dissipated power and the percentage of each element and each type of flux.

These partial power balances can be summarized as follows. In case of plasma off, most of the power is reflected and only a small fraction heats up the microwave circuit. In average, only 6 % of the power is missingin the power balance. This power may be found in MW leaks and in the capillary heat. However, we should remind that error bars of MW power measurements are sufficient to explain the missing 6 %.When the plasma is on, surprisingly, only 47 % of input power is coupled into plasma, in average, including the MW leaks. This result will be discussed in Section 3.8.

3.4 Heat dissipated by the capillary

As underlined above, the heat dissipated by the capillary represents a power fraction that is truly coupled to plasma. This is assessed based on capillary temperature surface measurements and by integrating over the capillary surface equations (3) and (4). For the incident power of 15 W,about 2 to 3 W are measured as conducto-convective and thermal radiative powers in fractions of 2/3 and 1/3, respectively (see table 3). So, the highest power corresponds to the lowest flow, for which the plasma is the longest, these powers representing between 13 to 20 % of the incident power.

Ar flow	Power	(%)	
Nml/min	*W*	φ^{CC}	φ^{R}
300	2.79	64	36
500	2.64	67.6	32.4
700	1.92	71.1	28.9

Table 3. Plasma on, the capillary dissipated power and the percentage of each type of flux.

3.5 MW power leaks

The MW power at 2.45 GHz can leak from the launcher at insertion holes where the capillary passes through the system. No leaks are expected for the rest of the circuit that are metallic enclosures. To quantify the MW leaks an electromagnetic probe (Electrosmogmeter,

TES-593) was employed. It works in the spectral range of 10 MHz to 8 GHz and evaluates the amplitude of the EM flux vector at the given location probing its three components. The manufacturing calibration factor specific for 2.45 GHz was implemented. The EM flux values were given in $\mu W/cm^2$. The value reported here at each location was averaged over a few seconds and the background EM noise was found to be zero when the MW power was switched off.

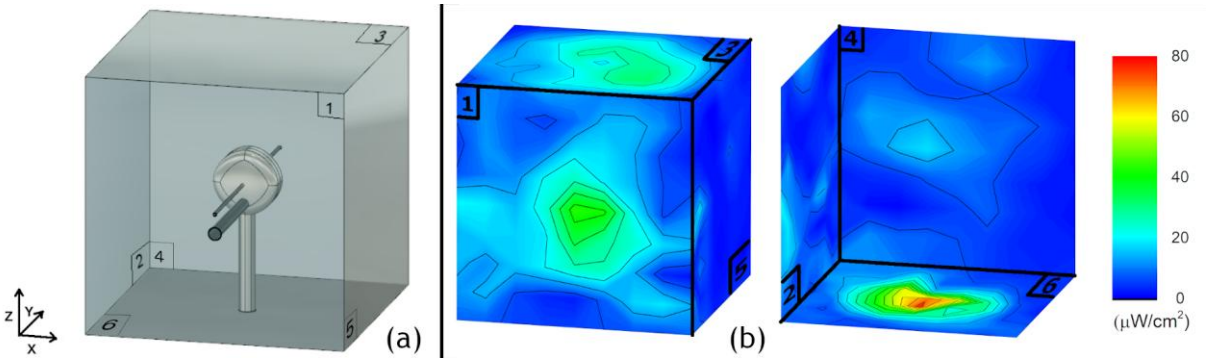

Figure 7. Virtual cube geometry (a) and the MW flux values measured over the six surfaces surrounding the launcher, in absence of the capillary and for 20 W input power (b).

To determine the MW leak power, EM flux measurements were performed over the surface of a virtual cube of 40 x 40 x 40 cm^3 having the stripline placed at the center, as shown in figure 7 (a). The distance between locations was 5 cm. The experiments were carried out in absence of plasma and capillary, to reduce MW reflections forincident and reflected powers of 20 W and 13 W, respectively. We should note that room walls where at about 5 m distance and the only MW reflective surfaces were the optical table placed at 10 cm below the bottom surface of the virtual cube and the MW coaxial cable. The flux measurements crossing the 6 surfaces of the cube are shown in figure 7 (b). The averaged fluxes through the six surfaces are comparable within a factor 4, namely 12.9, 6.9, 15.4, 6.3, 3.9 and 15 $\mu W/cm^2$. Integrating the MW flux over the virtual surface gives 95.5 mW for the leak power, which is below 0.5 % of the incident power.

In figure 8 we compared the EM flux field crossing surface 1without plasma for 40 W and 27 W, incident and reflected powers, respectively, and with the case of an Ar jet plasma of 20 W and 7 W, incident and reflected powers, respectively. We remark that the corresponding averaged fluxes are still comparable, namely 12.9, 20.7 and 10.5 $\mu W/cm^2$. These measurements demonstrated that the MW leaks are negligible also in presence of plasma, being on the order of 0.5 % or below.

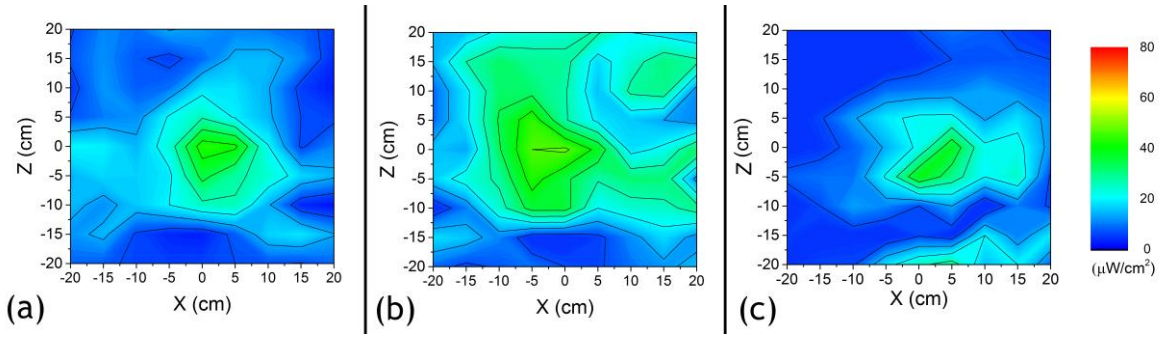

Figure 8. MW flux field crossing surface 1: no plasma, no capillary incident and reflected power 20 W and 13 W, respectively (a); no plasma, incident and reflected powers 40 W and 27 W, respectively (b); *right* - plasma jet argon, incident and reflected powers 20 W and 7 W, respectively (c).

3.6 Optical power emitted by plasma

As explained, a part of the plasma power will be transferred by radiation across the capillary, which is transparent in the spectral domain 0.2 to 3.6 μm. To estimate this contribution, an optical system made by two convergent lenses of 15 cm focal was employed. The collected light was focused on a fiber equipped with a pin hole of 50 μm. By aligning the system perpendicular to the capillary axis, the collected volume was selected to be a cylinder of about 50 μm diameter and 1 mm length, which corresponds to the capillary internal diameter. The fiber transmitted then the light to a spectrometer (Ocean Optics, Maya 2000 pro), which records spectra in the range of about 300 to 900 nm with 10 ms integration time and 50 samples averaging. The collection system was translated axially along the plasma emission region with a space resolution down to 1 mm. The spectra in arbitrary units were converted in absolute intensity units (i.e. $W/m^2/sr/nm$) using a standard calibration sphere (Gooch&Housego, OL 455-4-2), which was placed at the focal point of the collection system. In figure 9 a calibrated sample of Ar plasma spectrum is given.

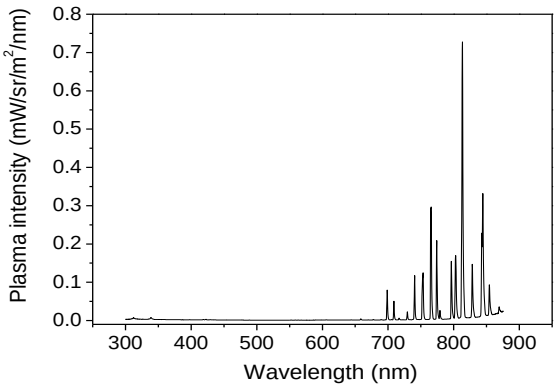

Figure 9. Sample of plasma intensity absolute emission spectrum calibrated using a standard source.

The radiance, which represents the spectral integrated intensity is plotted as a function of the axial position in figure 10. The gray region represents the part of the capillary tube covered by the launcher. As described above, by integrating the plasma emission coefficient over the spectral region, plasma volume and solid angle, the optical radiative power is determined to be a few microwatts, which is negligible here for the plasma power balance.

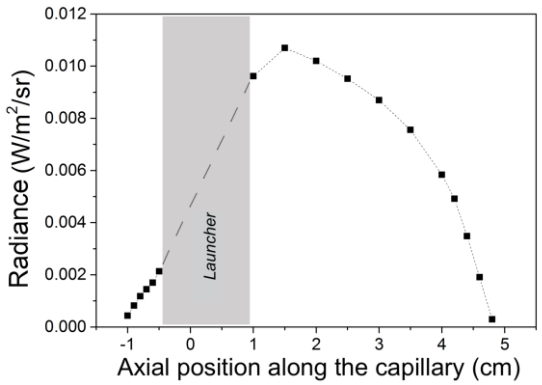

Figure 10. Radiance as a function of the axial position of the plasma region.

3.7 Post-discharge convective and chemical powers

Outside the plasma region, at the capillary exit (gas flow exhaust), the post-discharge convects heat to the ambient air. Moreover long-life non-radiative excited state species, namely Ar metastables, can contain a fraction of the injected power. These two channels are discussed below.

As mentioned above, the gas tempeature is measured by a thermocouple (Omega engineering, type K) of 50 μm diameter, placed a few centimeters downstream from the emissive plasma region, where the capillary surface temperature is about the room temperature. The post-discharge gas temperature in the dowstream can change significantely

compared to the upstream incoming Ar flow (e.g. $\Delta T \leq 100$ °C). It varies strongly with power, flow and launcher position. However, even for the highest temperature, the power in the thermal convective flux evaluated by Eq (5) stays always below 10 mW. This is less than 0.1 % of the incident power, therefore negligible in the present power balance.

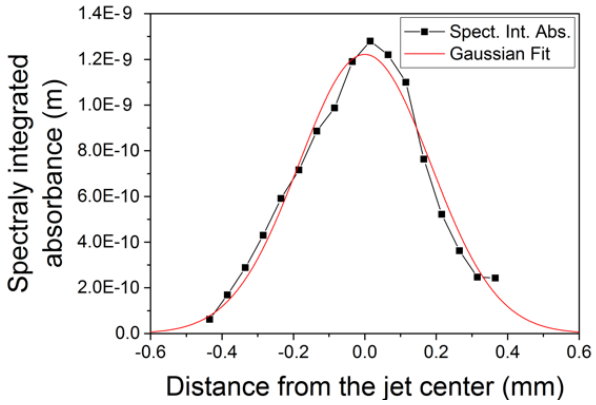

Figure 11. Spectral integrated absorbance of Ar^{met} as a function of distance from the plasma jet center.

The chemical power, i.e. the power involved in the gas reactivity, is reduced in present experiment to only one species because we employed argon, an inert gas. All the excited states produced by the discharge deexcite fast (radiative lifetimes ~ tens of ns), except two lower states for which the transition to the ground state is forbidden by the quantum mechanics selection rules. These states are called metastable and they survive much longer times. In the case of Ar metastables, their lifetime can be in the range of seconds.

To estimate the convective flux of Ar metastables, accordingto Eq (6), the density and convective speed are required. The flow speed can be determined from the mass flow rate and the capillary cross-section (i.e. below 10 m/s), whereas the Ar metastable density was measured by Tunable Diode Laser Absorption Spectroscopy (TDLAS), for details see reference[22]. Due to the presence of the capillary, *in situ* measurements in exactely the same conditions could not be performed. Instead, the Ar metastable density was measured in the jet configuration at atmospheric pressure at 50 μm at the capillary exit for 40 W power.The laser was tuned over 40 pm around 801.698 nm to probe the metastable level $3s^2 3p^5(^2P°_{3/2})4s$, which lies at 11.55 eV. The laser spot was reduced to of about 50 μm diameter, fine enough to ensure sufficient spatial resolution that is necessary for 1 mm diameter plasma jet. The spectraly integrated absorbance measured across the jet diameter with its Gaussian fit is shown in figure 11. These data are then converted in absolute density by Abel inversion and give a peak density of $5x10^{12} cm^{-3}$, which corresponds to a fraction of 0.2 ppm at atmospheric pressure and with a FWHM of 4 mm. With this density distribution the power present in the

convective Ar^{met} flux is estimated to be tens of microwatts, so orders of magnitude less than the incident power, and therefore negligible in the power balance.

However, we may argue that Ar^{met} leaves longer in the post discharge at 10 mbar. Nonetheless, even when assuming one hundred percent of Ar^{met}, the power present in the convective flux is estimated to be tens of milliwatts, so still negligible in the power balance. Yet in case of molecular gases, the chemical power could be significantly different and this type of analysis should be carrefully performed.

4.Power balance summary and discussions

In figure 12 the power fractions determined in absence of plasma are presented. As shown, most of the power is reflected back to the microwave generator due to the impedance mismatching, and over 5% heats up the MW circuit. One can remark that about 6.5 % is not measured. This small fraction may be due to underestimation of heat losses of the MW circuit. However, it could be also due to imprecision of the incident and reflected power measurements (see discussions below).

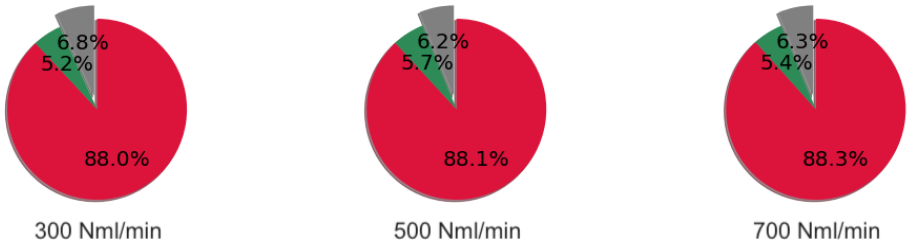

Figure 12. Plasma off, power fractions represented for three argon flow conditions: (red) reflected power, (green) power dissipated by microwave circuit, (gray) non-measured power.

In figure 13 the power fractions in case of plasmas for flows of 300, 500, and 700 Nml/min and 5W, 10W and 15W are shown. Here we observe the following. *(i)* The fraction of power going into the plasma is systematically higher when the injected MW power increases. This is due to a better impedance matching of the MW launcher. There is a significantly lower reflected power at 15W compared to 10W and 5W, in average 29 % compared to 37 % and 44 %, respectively. *(ii)* The fraction of power going into the plasma increases systematically when the gas flow decreases. This,again, is due to a better impedance matching. There is a significantly lower reflected power at 300 Nml/min compared to 500 Nml/min and 700 Nml/min, in average 34% compared to 37% and 39 %, respectively. *(iii)* As shown in figure 13, the non-measured power fraction is about 30 % of the incident power.

This unknown fraction is significantly higher than for the plasma case, where only 6.5 % is not measured. No systematic trends with reflected power fractions (with impedance matching) are observed. Although this power fraction is important, it can be explained by measurement uncertainties. We should recall that the bidirectional coupler is quoted with an attenuation of 30(±1.2) dB on the power measurement channels. This explains easily the missing 6.5 % in the plasma off experiment and within attenuator precisions even the missing 30 % can be justified. The correlation uncertainties are expected to be also important, particularly for determination of the conducto-convective coefficient employed for capillary flux assessment.

Thus, according to figure 12, the real power coupled to the system should be reduced by about 6.5 %. It comes out that the power fraction coupled to the plasma, after this correction, lies in a range between 4 % to 20 % in our experiments. Note that this is far below the 95% that is measured here based on the generator display (incident minus reflected power). Because the experimental uncertainties are significant, the plasma fractions could be underestimated here, in particular for low-power experiments. However, even considering all the missing power to be absorbed by plasma, the fraction of plasma power will range in the upper most case between 28% and 47 %, for input powers between 5 W and 15 W. For the corresponding typical plasma lengths of 3 cm and 7 cm, respectively and 1 mm capillary diameter, the upper bound for the averaged power densities is estimated as 60 Wcm^{-3} and 130 Wcm^{-3}, respectively.

In summary, the power coupled to the plasma in our microwave capillary discharges is at least a factor of 2 smaller than the value indicated by the generator (assuming the non-measured power fraction to be coupled to the plasma). In the other extreme limit, it is overestimated by a factor about 20 (the non-measured fraction does not contribute to maintain the plasma). Yet, this last factor corresponds to measurements at 5W, where the capillary temperature is closer to the room temperature, so the thermal flux measurement is prone to a larger systematic underestimation. Therefore, this number should be regarded with reservations.

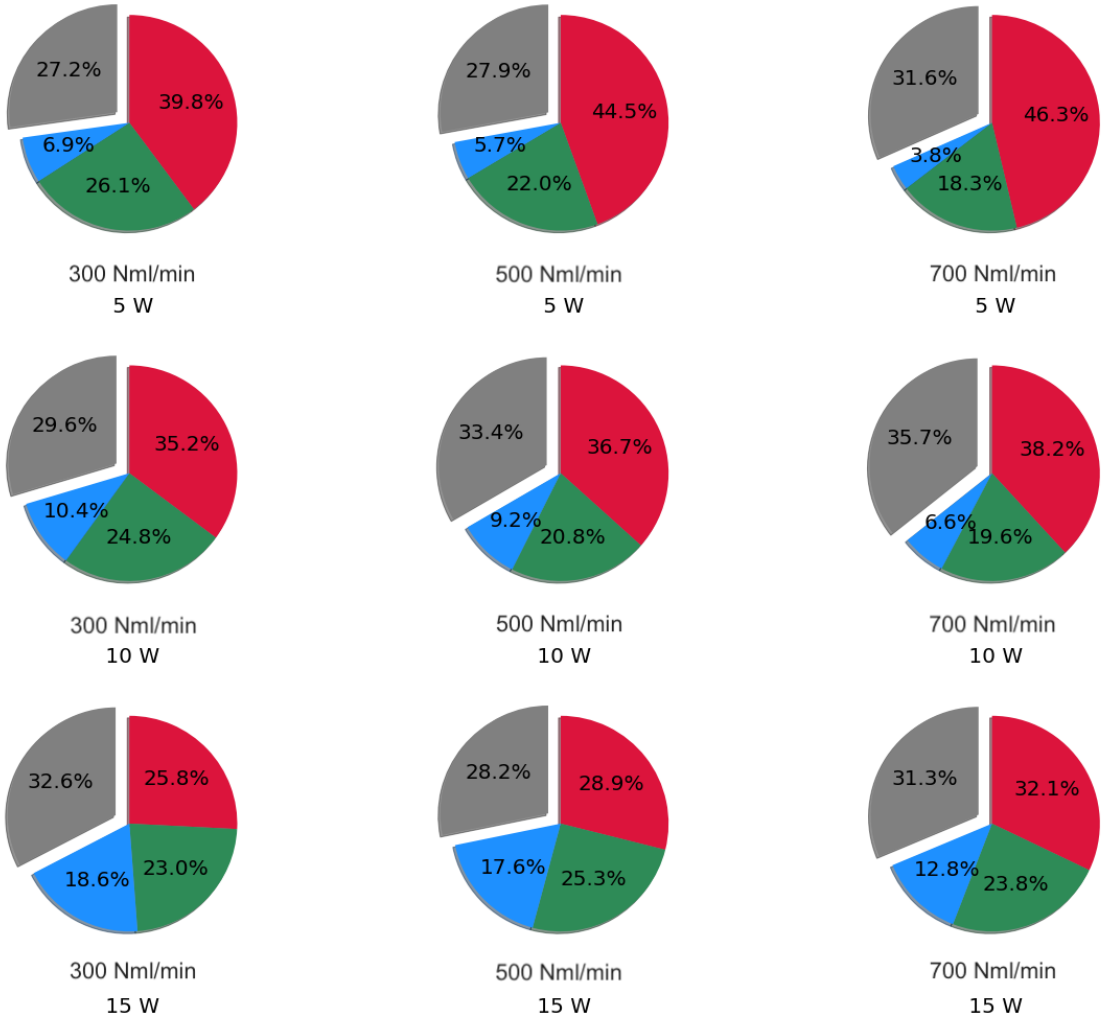

Figure 13. Plasma on conditions, power fractions represented for different argon flows and incident powers: (red) reflected power, (green) power dissipated by microwave circuit, (gray) non-measured power, (blue) power dissipated by capillary(plasma power).

5. Conclusions

The macroscopic power balance was performed in microwave capillary discharges under controlled argon flows and microwave powers at atmospheric and intermediate pressures. The applied methodology was described in detail. The power balance was experimentally performed based on measurements of MW incident and reflected powers, MW leak fluxes, heat fluxes across the capillary and MW launcher and convective heat and chemical fluxes at capillary exit. An infrared camera, thermocouples and thermal sensitive papers were used to accurately determine the surface and gas temperatures and subsequently the conducto-convective, convective and thermal radiative fluxes and their corresponding powers. The TDLAS technique was employed to measure Ar metastable densities in the post

discharge, whereas the calibrated OES technique was used to evaluate the optical radiative power.

After gathering all these power fractions, the power coupled effectively to the capillary plasma was determined. Its value was found to range from 4 % to 20 %, which is much less than values reported in the literature (i.e.typically over 90%) based on the injected and reflected powers displayed by the generator. Within the experimental errors, it was demonstrated that power coupled in these plasmas is at least a factor 2 overestimated by the common reported method.

Negligible power fractions (< 1%) were found for the optical radiation transmitted through the capillary, the gas heating and excitation energy at capillary exit, and the MW leaks at the launcher gap. The power coupled to the argon plasma was mainly converted in the heat flux across the capillary. Within instrumental accuracies the power balance obtained from incident and reflected powers measured near the launcher, was found as the sum of heating powers of the microwave circuit (includes a launcher, N-type connectors,a bi-directional coupler) and capillary tube.

The present power assessment is particularly important for small plasma volumes such as micro-discharges, where, although the injected power remains low (typically a few watts), the power density can exceed 10^5 Wcm^{-3}. Further improvements of the plasma power balance require more accurate equipment, in particular for the microwave circuit (coupler, attenuators), superior precision on temperature measurements, and the generation of larger plasma volumes using higher MW powers in capillary cooled systems, conditions for which the heat transfer could be better determined and controlled. A more complex approach is necessary in case of hotter plasmas, as the thermal radiation spectrum shifts to the capillary transparent spectral regions. The present methodology could be applied to reactive capillary plasmas, here in addition atomic and molecular fluxes need to be evaluated at capillary exit, and to other sources of plasmas (e.g. atmospheric pressure jets), especially those presenting heated walls.

Acknowledgements. This research was founded by Labex LaSIPS, University Paris-Saclay, THERMOPLAS project RD 73.

References

[1] Mariotti D and Sankaran R M 2010 Microplasmas for nanomaterials synthesis *J. Phys. D. Appl. Phys.***43** 323001

[2] Takao Y, Ono K, Takahashi K and Eriguchi K 2006 Plasma diagnostics and thrust performance analysis of a microwave-excited microplasma thruster *Jpn. J. Appl. Phys.***45** 8235–40

[3] Debord B, Jamier R, Gérôme F, Leroy O, Boisse-Laporte C, Leprince P, Alves L L and Benabid F 2013 Generation and confinement of microwave gas-plasma in photonic dielectric microstructure *Opt. Express***21** 025509

[4] Pilla G, Galley D, Lacoste D A, Lacas F, Veynante D and Laux C O 2006 Stabilization of a Turbulent Premixed Flame Using a Nanosecond Repetitively Pulsed Plasma *IEEE Trans. Plasma Sci.***34** 2471–7

[5] Stancu G D, Kaddouri F, Lacoste D A and Laux C O 2010 Atmospheric pressure plasma diagnostics by OES, CRDS and TALIF *J. Phys. D. Appl. Phys.***43** 124002

[6] Miclea M and Franzke J 2007 Analytical detectors based on microplasma spectrometry *Plasma Chem. Plasma Process.***27** 205–24

[7] Graves D B 2014 Low temperature plasma biomedicine: A tutorial review *Phys. Plasmas***21** 080901

[8] Adamovich I, Baalrud S D, Bogaerts A, Bruggeman P J, Cappelli M, Colombo V, Czarnetzki U, Ebert U, Eden J G, Favia P, Graves D B, Hamaguchi S, Hieftje G, Hori M, Kaganovich I D, Kortshagen U, Kushner M J, Mason N J, Mazouffre S, Thagard S M, Metelmann H-R, Mizuno A, Moreau E, Murphy A B, Niemira B A, Oehrlein G S, Petrovic Z L, Pitchford L C, Pu Y-K, Rauf S, Sakai O, Samukawa S, Starikovskaia S, Tennyson J, Terashima K, Turner M M, van de Sanden M C M and Vardelle A 2017 The 2017 Plasma Roadmap : Low temperature The 2017 Plasma Roadmap : Low temperature plasma science and technology *J. Phys. D. Appl. Phys.***50** 323001

[9] Ferreira C M and Moisan M 1993 *Microwave discharges fundamentals and applications* (Nato ASI Series B: Physics vol. 302,Springer Science+Business Media New York)

[10] Dap S, Leroy O, Andrieu J, Boisse-Laporte C, Leprince P, Stancu G D and Minea T 2015 Hydrodynamic and thermal effects of continuous microwave-sustained plasma in capillary tubes *Plasma Sources Sci. Technol.***24** 65007

[11] Debord B, Alves L L, Gérôme F, Jamier R, Leroy O, Boisse-Laporte C, Leprince P and Benabid F 2014 Microwave-driven plasmas in hollow-core photonic crystal fibres *Plasma Sources Sci. Technol.***23** 015022

[12] Stancu G D, Leroy O, Coche P, Gadonna K, Guerra V, Minea T and Alves L L 2016 Microwave air plasmas in capillaries at low pressure II. Experimental investigation *J.*

*Phys. D. Appl. Phys.***49** 435202

[13] Glaude V M M, Moisan M, Pantel R, Leprince P and Marec J 1980 Axial electron density and wave power distributions along a plasma column sustained by the propagation of a surface microwave *J. Appl. Phys.***51** 5693–8

[14] Chaker M, Nghiem P, Bloyet E, Leprince P and Marec J 1982 Characteristics and energy balance of a plasma column sustained by a surface wave *J Phys. Lettres***43** L-71-L75

[15] Sugai H, Ghanashev I and Nagatsu M 1998 High-density flat plasma production based on surface waves *Plasma Sources Sci. Technol.***7** 192–205

[16] Durocher-Jean A, Delnour N and Stafford L 2019 Influence of N2, O2, and H2 admixtures on the electron power balance and neutral gas heating in microwave Ar plasmas at atmospheric pressure *J. Phys. D. Appl. Phys.***52** 475201

[17] Hemawan K W, Keefer D W, Badding J V and Hemley R J 2016 Generation of Microwave Capillary Argon Plasmas at Atmospheric Pressure *IEEE Trans. Plasma Sci.***44** 2603–7

[18] P Coche V G and L L A 2016 Microwave air plasmas in capillaries at low pressure I. Self-consistent modeling *J. Phys. D. Appl. Phys.***49** 235207

[19] Whitaker S 1977 *Fundamental Principles of Heat Transfer* (Pergamon Press INC)

[20] Gillespi D, Olsen A L and Nichols L W 1965 Transmittance of Optical Materials at High Temperatures in 1-u to 12-u Range *Appl. Opt.***4** 1488

[21] Roberts S and Coon D D 1962 Far-Infrared Properties of Quartz and Sapphire *J. Opt. Soc. Am.***52** 1023

[22] Vitelaru C, Lundin D, Stancu G D, Brenning N, Bretagne J and Minea T 2012 Argon metastables in HiPIMS: Time-resolved tunable diode-laser diagnostics *Plasma Sources Sci. Technol.***21** 025010

[23] Churchill S W and Chu H H S 1975 Correlating equations for laminar and turbulent free convection from a horizontal cylinder *Int. J. Heat Mass Transf.***18** 1049–53

[24] Churchill S W and Chu H H H S 1975 Correlating equations for laminar and turbulent free convection from a vertical plate *Int. J. Heat Mass Transf.***18** 1323–9

[25] Lloyd J R and Moran W R 1974 Natural Convection Adjacent To Horizontal Surface of Various Planforms. *J Heat Transf.***96** 443–7

[26] McAdams W H 1954 *Heat Transmission* (McGraw-Hill, New York)

[27] Http://www.nist.gov *http://www.nist.gov*

[28] Efimova V, Derzsi A, Zlotorowicz A, Hoffmann V, Donkó Z and Eckert J 2010

Influence of the anode material on the characteristics of an analytical glow discharge cell *Spectrochim. Acta - Part B At. Spectrosc.***65** 311–5

[29] Jones J M, Mason P E and Williams A 2019 A compilation of data on the radiant emissivity of some materials at high temperatures *J. Energy Inst.***92** 523–34

[30] Maturilli A and Helbert J 2014 Characterization, testing, calibration, and validation of the Berlin emissivity database *J. Appl. Remote Sens.***8** 084985

[31] Moisan M, Pantel R, Hubert J, Bloyet E, Leprince P, Marec J and Richard A 1979 Production and Applications of Microwave Surface Wave Plasma At Atmospheric Pressure. *J. Microw. Power***14** 57–61